JOURNAL OF CATALYSIS **171,** 148–159 (1997)
ARTICLE NO. CA971775

Non-Faradaic Electrochemical Modification of Catalytic Activity

11. Ethane Oxidation on Pt

Anthony Kaloyannis and Constantinos G. Vayenas

Department of Chemical Engineering, University of Patras, GR-26500 Patras, Greece

Received January 31, 1997; revised May 19, 1997; accepted June 2, 1997

The rate of ethane oxidation on polycrystalline Pt catalyst films deposited on 8 mol% Y_2O_3-stabilized ZrO_2, an O^{2-} conductor, can be reversibly enhanced by up to a factor of 20 by varying the potential of the Pt film. The rate increase is typically a factor of 200 higher than the electrochemically controlled rate of supply of promoting oxide ions. Electrochemical oxygen removal from the Pt catalyst surface also enhances the catalytic rate by up to a factor of 7. In this case the rate increase is typically a factor of 20 higher than the electrochemically controlled rate of oxygen removal. The ethane oxidation activation energy varies linearly by a factor of 3 with varying catalyst potential, leading to the appearance of the compensation effect. The observed pronounced promotional phenomena are discussed on the basis of the reaction mechanism, previous electrochemical promotion studies and recent TPD and XPS investigations.

INTRODUCTION

During the past 8 years the effect of non-Faradaic electrochemical modification of catalytic activity (NEMCA) (1–3), or electrochemical promotion (4) or *in situ* controlled promotion (5), has been described for over 40 catalytic reactions on Pt, Pd, Rh, Au, Ag, Ni, and IrO_2 catalysts using O^{2-}-conducting solid electrolytes, such as yttria-stabilized zirconia (YSZ) (1–3); Na^+-conducting solid electrolytes, such as β''-Al_2O_3 (5, 6); H^+ conducting solid electrolytes, such as $CsHSO_4$ (7), $CaZr_{0.9}In_{0.1}O_{3-a}$ (8) and Nafion (9); F^- conducting solid electrolytes, such as CaF_2 (10); and mixed ionic–electronic conductors, such as TiO_2 (11) as the active catalyst support. The effect has also been recently studied in aqueous electrolyte systems (12–14). Work in this area has been reviewed extensively (15–17).

The porous metal or metallic oxide (18) catalyst film serves simultaneously as an electrode in the galvanic cell

gaseous reactants, metal catalyst|solid electrolyte|metal, O_2

and the NEMCA effect is induced by applying currents or potentials (typically -2 to $+2$ V) between the catalyst and the metal counter electrode. When using YSZ as the solid electrolyte the induced increase in catalytic rate is up to 3×10^5 times larger than the rate, $I/2F$, of O^{2-} supply to the catalyst (2, 15–17) (where I is the applied current and F is Faraday's constant) and up to 100 times larger than the catalytic rate when no current is applied (18).

Three parameters are commonly used for the macroscopic description of electrochemical promotion:

1. The enhancement factor or Faradaic efficiency, Λ, defined by

$$\Lambda \equiv \Delta r/(I/2F), \qquad [1]$$

where Δr is the induced change in catalytic rate expressed in mol O/s. The current, I, is defined positive when anions are supplied to the catalyst. A reaction exhibits the NEMCA effect when $|\Lambda| > 1$. When $\Lambda > 1$ the reaction is termed electrophobic, while when $\Lambda < -1$ the reaction is termed electrophilic. As shown both experimentally and theoretically (15–17) the order of magnitude of the absolute value, $|\Lambda|$, of the Faradaic efficiency Λ can be estimated for any reaction, catalyst, or solid electrolyte from

$$|\Lambda| \approx 2Fr_o/I_o, \qquad [2]$$

where r_o is the open-circuit (unpromoted) catalytic rate and I_o is the exchange current of the electrocatalytic (charge-transfer) reaction at the catalyst–solid electrolyte interface. Equation [2] dictates that in order to obtain a non-Faradaic rate enhancement ($|\Lambda| > 1$) it is necessary to have a catalytic reaction intrinscically faster than the corresponding electrocatalytic reaction, i.e., $r_o > (I_o/2F)$.

2. The rate enhancement ratio, ρ, defined by

$$\rho = r/r_o. \qquad [3]$$

3. The promotion index PI_i of the promoting ion, i, defined by

$$PI_i = \frac{\Delta r/r_o}{\Delta\theta_i}, \qquad [4]$$

where θ_i is the coverage of the promoting species (e.g., $O^{\delta-}$, $Na^{\delta+}$) on the catalyst surface. When the promoting species

0021-9517/97 $25.00

does not react appreciably with any of the reactants (e.g., $Na^{\delta+}$) then its coverage, θ_i, can be measured accurately on the catalyst surface via coulometry (5, 6), and thus PI_i can be easily computed (5, 6); PI_{Na} values up to 3000 have been measured for the NO reduction by H_2 on Pt (20). When the promoting species (e.g., $O^{\delta-}$) is also partially consumed by one of the reactants, as in the present case (where C_2H_6 reacts with the promoting species $O^{\delta-}$ at a rate Λ times smaller (19) than with normally chemisorbed oxygen), then the measurement of PI_i is less accurate. In such cases a conservative estimate of PI_i can be obtained from $PI_i = (\Delta r/r_o)_{max}$, i.e., by assuming that the maximum rate enhancement is obtained for $\Delta\theta_{O^{\delta-}} = 1$ (16, 21). A more precise method for measuring $\theta_{O^{\delta-}}$, and thus $PI_{O^{\delta-}}$, is given in the present work.

Recent XPS (21–23), SERS (24, 25), cyclic voltammetric (26), TPD (26), and STM (27) investigations have shown that, as originally proposed on the basis of rate transients (2, 15), the NEMCA effect is due to an electrochemically controlled migration (backspillover) of ionic species from the solid electrolyte onto the gas-exposed catalyst-electrode surface. These backspillover ionic species alter the catalyst surface work function, $e\Phi$, by

$$\Delta(e\Phi) = e\Delta V_{WR}, \qquad [5]$$

where V_{WR} is the catalyst (working electrode, W) potential with respect to the reference (R) electrode (3, 28, 29). Electrochemical promotion is thus due to the promoting action of these backspillover species ($O^{\delta-}$ in the case of YSZ, $Na^{\delta+}$ in the case of β''-Al_2O_3) which affect the binding strength of chemisorbed reactants and intermediates via through-the-metal and through-the-vacuum interactions (15–17). Recent *ab initio* quantum mechanical calculations using metal clusters and oxygen atoms coadsorbed with ions or point charges have confirmed this picture and have provided a firm theoretical basis for a fundamental understanding of electrochemical promotion and more generally of promotion on metal catalysts (30).

The nature of the promoting $O^{\delta-}$ species on Pt interfaced with YSZ has been investigated with XPS (21), SERS (24), cyclic voltammetry (26), and TPD (26). The XPS investigation has shown that its O1*s* binding energy is at 528.8 eV (21). The TPD investigation has shown that its peak desorption temperature is at $T_p \approx 750$–780 K vs $T_p \approx 675$–685 K for weakly bonded atomic oxygen (O1*s* binding energy at 530 eV (21)) which coexists on the Pt surface and is displaced to this weakly bonded state from its normal chemisorptive state ($T_p \approx 720$–730 K) by the coadsorbed strongly bonded $O^{\delta-}$ species (26).

The complete (31–34) and partial (34, 35) oxidation of ethane has been investigated on several metal oxide (31, 32, 34, 35) and metal (33, 36) surfaces including Pt (36). The ethane dissociation dynamics on Pt(111) have been studied in detail by McMaster and Madix (37), who found that the initial step for ethane dissociation involves C–H bond cleavage. Molecular ethane adsorption is weak (37, 38) and thus dissociative ethane chemisorption, which is a structure-sensitive process (37, 38), is likely to be the first step for ethane oxidation on Pt (37).

In this work we study the effect of electrochemical promotion for ethane oxidation on polycrystalline Pt deposited on YSZ. Similarly with the cases of C_2H_4 (2) and C_3H_6 (39) oxidation on Pt/YSZ, ethane oxidation is found to exhibit a pronounced electrophobic NEMCA enhancement with positive currents, i.e., $O^{\delta-}$ supply to the catalyst. Interestingly it is found that the reaction also exhibits a strong electrophilic enhancement with negative currents, i.e., with removal of atomic oxygen from the catalyst surface.

EXPERIMENTAL

The atmospheric pressure continuous flow apparatus has been described previously (6, 11, 15, 19, 39). Reactants were Messer Griesheim certified standards of C_2H_6 in He and O_2 in He. They could be further diluted in ultrapure (99.999%) He. Reactants and products were analyzed by on-line gas chromatography (Perkin–Elmer Sigma 300) with a TC detector and Perkin–Elmer LCI-100 computing integrator. A Porapak N column was used to separate O_2, C_2H_6, CO_2, and H_2O. No other products were detected. The CO_2 concentration in the reactor effluent was also continuously monitored using an Anarad Infrared CO_2 analyzer.

The well-mixed quartz reactor of volume 30 cm^3 was of the single-pellet type (40, 41); i.e., the YSZ disc (19 mm diameter, 2 mm thickness) was suspended in the quartz tube (Fig. 1a) with three Au wires attached to the catalyst, counter, and reference electrodes.

The Pt catalyst film (mass 3 mg, superficial surface area 1.05 cm^2) was deposited on one side of the YSZ disc using a thin coating of unfluxed Engelhard A1121 Pt paste followed by drying and calcination in air, first for 2 h at 400°C, then for 1 h at 800°C (Fig. 1b). The true surface area of the Pt film was determined by measuring its reactive oxygen uptake at 380°C via the isothermal titration technique: The Pt film is first exposed to O_2 for several min and then the reactor is purged with ultrapure He for a time t_{He}, several times longer than the reactor residence time to remove gaseous O_2. Subsequently the reactor is purged with CO and the amount of oxygen, N, remaining on the surface is obtained by integrating the area of the CO_2 peak in the reactor effluent. By varying t_{He} one can study the kinetics of oxygen desorption (15–17). By extrapolating N to $t_{He} = 0$, one obtains the reactive oxygen catalyst uptake N_O. Figure 2 shows the results of the surface titration measurements. The reactive oxygen uptake is $N_O = 1.1 \times 10^{-6}$ mol O. Assuming a maximum oxygen coverage

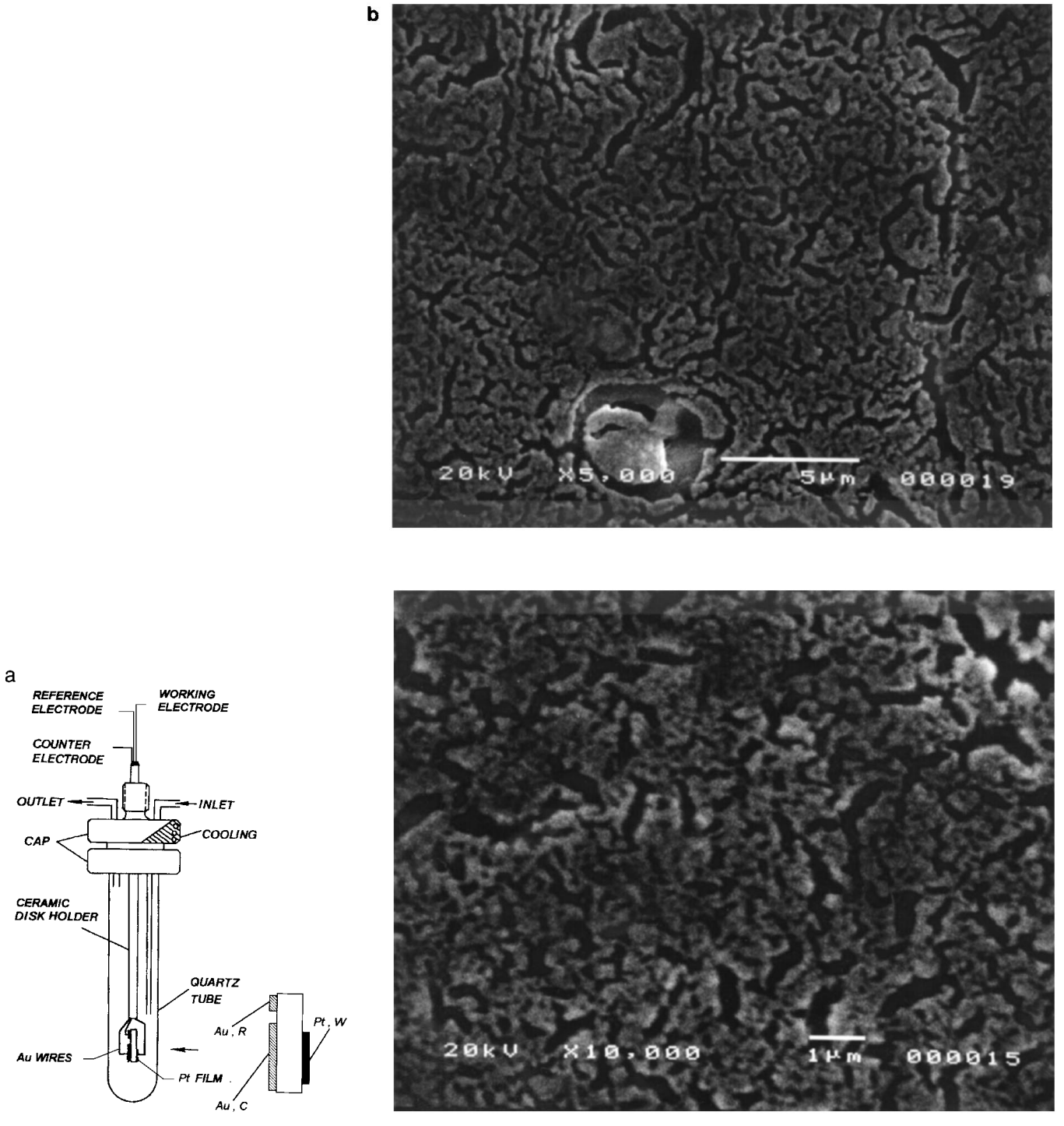

FIG. 1. (a) Single pellet catalytic reactor and three-electrode configuration. (b) Scanning electron micrographs of the Pt catalyst electrode.

of 0.25 (27) this corresponds to a true Pt surface area of 1800 cm^2.

Gold counter and reference electrodes were deposited on the other side of the disc using thin coatings of a Au paste prepared from a slurry of Au powder (Aldrich Chemicals) in ethyl acetate followed by calcination in air at 810°C for 10 min. Au was chosen as the auxiliary electrode material because of its inertness for C_2H_6 oxidation (checked via blank experiments) which makes it an adequate pseudoreference electrode when using the single pellet design, as discussed recently (42). Thus to a good approximation (±0.1 V) (42) the measured open-circuit potentials, V^o_{WR},

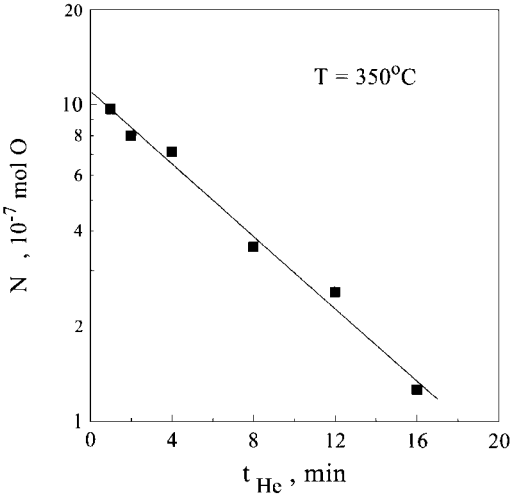

FIG. 2. Isothermal titration of surface oxygen with CO. Effect of oxygen desorption time, t_{He}, on the mass of reactive oxygen on the Pt catalyst surface.

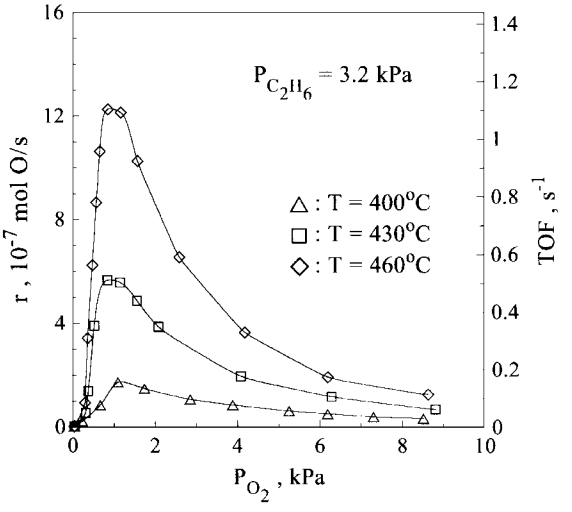

FIG. 3. Effect of P_{O_2} and temperature on the rate and turnover frequency of ethane oxidation.

but also the imposed potentials V_{WR} can be referenced to the equilibrium potential of oxygen corresponding to the oxygen partial pressure in the reactive gas mixture. The open-circuit potential, V^o_{WR}, in presence of $P_{O_2} = 21$ kPa was very near the theoretical value of zero (∼0.05 V) over the temperature range of the present investigation (400–500°C). The origin of such small offset potentials at these relatively low temperatures has been discussed previously (15, 16).

RESULTS

Open-Circuit Kinetics

Figures 3 and 4 show the dependence of the rate, r, of ethane oxidation on the partial pressures, P_{O_2} and $P_{C_2H_6}$, of oxygen and ethane, respectively, under open-circuit, i.e., unpromoted, conditions. In these and subsequent figures the rate of ethane oxidation is expressed in mol O/s and also as turnover frequency (TOF), i.e., oxygen atoms reacting per surface site per second, by using the reactive oxygen uptake, $N_O = 1.1 \times 10^{-6}$ mol O, of the Pt catalyst film.

As shown in Fig. 3 the rate exhibits a pronounced maximum with respect to oxygen pressure at a P_{O_2} value, hereafter denoted $P^*_{O_2}$, which is weakly dependent on temperature. Figure 4 shows that the rate is positive order in ethane over the entire range of gaseous composition and temperature investigated in this work. The kinetics depicted in Figs. 3 and 4 suggest competitive adsorption of dissociatively chemisorbed oxygen and ethane (37) with stronger binding of oxygen than ethane on the catalyst surface, which leads to the appearance of the rate maximum at $P^*_{O_2}$. This is also corroborated by the fact that the open-circuit potential, V^o_{WR}, was found to be rather insensitive to $P_{C_2H_6}$. Thus varying $P_{C_2H_6}$ between 0 and 4 kPa at fixed P_{O_2} (0.6 kPa) was found to decrease V^o_{WR} by less than 0.1 V in contrast with previous studies of CO and C_2H_4 oxidation on Pt/YSZ (16) where P_{CO} and $P_{C_2H_4}$ values up to 2 kPa cause a pronounced, up to 0.4 V, decrease in V^o_{WR} under similar conditions. Therefore the V^o_{WR} values also suggest weak adsorption of ethane relative to oxygen.

Promotional Transients

Figures 5a and 5b show typical galvanostatic transients; i.e., they depict the catalytic rate and catalyst potential response upon application of a positive and of a negative current, respectively.

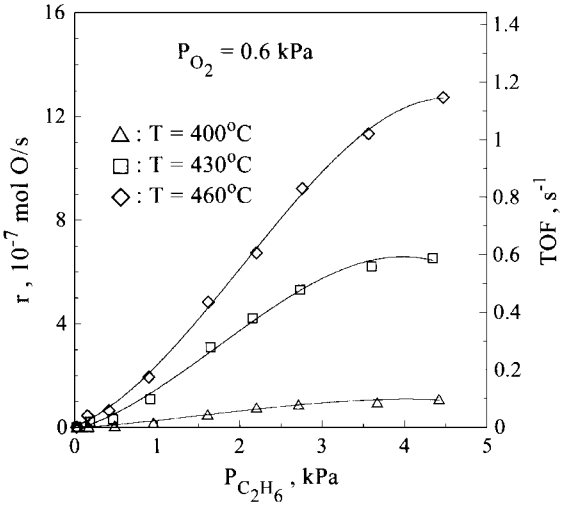

FIG. 4. Effect of $P_{C_2H_6}$ and temperature on the rate and turnover frequency of ethane oxidation.

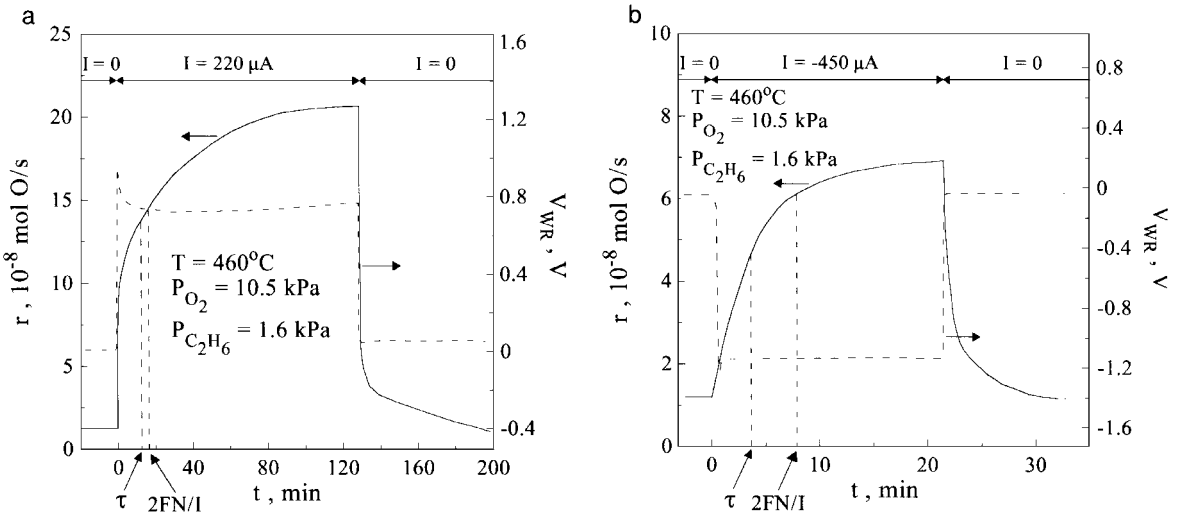

FIG. 5. Electrochemical promotion. Ethane oxidation rate (continuous line) and catalyst potential (dashed line) response to step changes in applied positive (a) and negative (b) current. The experimental (τ) and computed ($2FN/I$) rate relaxation time constants are also indicated. See text for discussion. $r_o = 1.25 \times 10^{-8}$ mol O/s, $P_{O_2} = 10.5$ kPa, $P_{C_2H_6} = 1.62$ kPa, $N = 1.1 \times 10^{-6}$ mol O.

The effect of positive current, $I = 220\ \mu$A, corresponding to the supply of $I/2F = 1.14 \times 10^{-9}$ mol O/s is shown in Fig. 5a. At $t \leq 0$ the circuit is open ($I = 0$) and the steady-state regular (unpromoted) catalytic rate is 1.25×10^{-8} mol O/s. Upon positive current application the rate increases by a factor of 15.5. The rate increase $\Delta r = 19.4 \times 10^{-8}$ mol O/s is 170 times larger than $I/2F$. This implies that each O^{2-} supplied to the catalyst causes, on the average, 170 chemisorbed oxygen atoms to react with ethane and form CO_2 and H_2O. Consequently for the galvanostatic transient of Fig. 5a the enhancement factor, or Faradaic efficiency, Λ, and rate enhancement ratio, ρ, equal 170 and 16.5, respectively:

$$\Lambda = \Delta r/(I/2F) = 170 \quad [6]$$

$$\rho = r/r_o = 16.5. \quad [7]$$

It is worth noting the very good agreement between the rate relaxation time constant τ (defined as the time required for the rate increase to reach 63% of its final steady-state value) and the parameter $2FN_O/I$, which is the time required to form a monolayer of promoting oxide ions (supplied at a rate $I/2F$) on the catalyst surface with N_O adsorption sites (Fig. 5a):

$$\tau \approx 2FN_O/I. \quad [8]$$

Upon current interruption both the catalytic rate and the catalyst potential return to their initial, unpromoted values showing the reversibility of *in situ* controlled promotion. It is worth noting that according to the analysis of electrochemical promotion transients outlined recently (19, 42), and presented under Discussion, the time constant, τ_S, of the rate transient upon current interruption reflects the kinetics of the reaction of the promoting oxide species with C_2H_6 and can be predicted by

$$\tau_S = \Lambda \cdot (TOF_p)^{-1}, \quad [9]$$

where TOF_p is the turnover frequency of the catalytic rate in the promoted state. Equation [9] reflects the fact that, for oxidation reactions, Λ expresses the ratio of the average lifetimes of the promoting oxide species and of normally chemisorbed oxygen on the catalyst surface (19). Thus for the transient of Fig. 5b it is $(TOF_p) = 0.19\ s^{-1}$, $\Lambda = 170$, and consequently from Eq. [9] one obtains $\tau_S = 15$ min, which is in very good qualitative agreement with the experimental τ_S value (Fig. 5a).

Figure 5b shows the effect of negative current application under the same temperature and gaseous composition as in Fig. 5a, thus starting from practically the same open-circuit (unpromoted) rate. Negative current application ($I = -450\ \mu$A corresponding to the removal of 2.33×10^{-9} mol O/s) causes a nearly fivefold enhancement in the rate ($\rho = 5.8$). The rate increase $\Delta r = 5.74 \times 10^{-8}$ mol O/s is 25 times larger than the rate ($-I/2F$) of oxygen removal. Consequently the Faradaic efficiency Λ equals $\Delta r/(I/2F) = -25$. The negative sign shows that the reaction exhibits electrophilic behavior (15, 17) upon negative current application, i.e.,

$$\Lambda < 0, \quad \partial r/\partial V_{WR} < 0, \quad PI_{O^{2-}} < 0 \quad [10]$$

in contrast with the electrophobic behavior (15–17) observed upon positive current application (Fig. 5a), i.e.,

$$\Lambda > 0, \quad \partial r/\partial V_{WR} > 0, \quad PI_{O^{2-}} > 0. \quad [11]$$

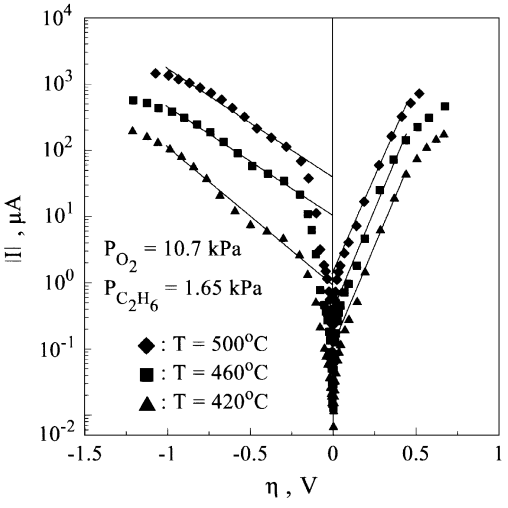

FIG. 6. Effect of catalyst overpotential $\eta(=V_{WR}-V^{o}_{WR})$ on the cell current.

Electrocatalytic Kinetics

Figure 6 shows the dependence of current, I, on catalyst overpotential, η. The latter is defined from

$$\eta = V_{WR} - V^{o}_{WR}, \qquad [12]$$

where V^{o}_{WR} is the open-circuit ($I=0$) catalyst potential. It is clear that the current-overpotential behavior is not symmetric for anodic ($I>0$) and cathodic ($I<0$) currents and thus cannot be described by a single value of the exchange current I_o in the Butler–Volmer equation

$$\ln(I/I_o) = \alpha_a F\eta/RT - \alpha_c F\eta/RT. \qquad [13]$$

This is because a single Butler–Volmer equation is satisfied only as long as the coverages of adsorbed species do not change appreciable with catalyst potential which is clearly not the case in most NEMCA studies (15–17). However, as shown in Fig. 6, the I vs η data can be adequately described for intermediate $|\eta|$ values by the Tafel equations

$$\ln(I/I_{o,a}) = \alpha_a F\eta/RT \qquad [14]$$

$$\ln(-I/I_{o,c}) = -\alpha_c F\eta/RT \qquad [15]$$

for anodic and cathodic operation, respectively. In these equations $I_{o,a}$, $I_{o,c}$ and α_a, α_c are the apparent anodic and cathodic exchange currents and transfer coefficients, respectively. Table 1 lists the extracted $I_{o,a}$, $I_{o,c}$, α_a, and α_c values. Both $I_{o,a}$ and $I_{o,c}$ increase exponentially with temperature with apparent activation energies of the order of 30 and 50 kcal/mol respectively, while α_a and α_c remain practically constant.

Steady-State Effect of Current on the Catalytic Rate

Figure 7 shows the steady-state effect of applied current, I, on the increase in the rate of ethane oxidation. The enhancement factor, or Faradaic efficiency, Λ, takes values between 100 and 500 for positive currents and between -10 and -100 for negative currents. The measured $|\Lambda|$ values are typically an order of magnitude smaller than those predicted by the approximate relationship

$$|\Lambda| \approx 2Fr_o/I_o \qquad [2]$$

as also shown in Table 1. It is worth noting, however, that despite this significant deviation, the measured Λ values show the same qualitative trends with the parameter $2Fr_o/I_o$; i.e., $|\Lambda|$ is larger in the anodic region where I_o is significantly smaller (Table 1).

TABLE 1

Electrokinetic Parameters and Open-Circuit Catalytic Rate ($P_{O_2}=10.7$ kPa, $P_{C_2H_6}=1.65$ kPa)

T (°C)	$I_{o,a}$ (μA)	$I_{o,c}$ (μA)	α_a	α_c	$r_o/(10^{-8}$ mol O/s)	$2Fr_o/I_{o,a}$	$2Fr_o/I_{o,c}$
420	0.11	0.95	0.81	0.29	0.68	11900	1380
460	0.37	10.63	0.87	0.25	1.27	6600	230
500	1.37	40.64	0.87	0.25	2.04	2870	97

Effect of Catalyst Potential

Figure 8 is based on the data of Figs. 6 and 7 and shows the dependence of the catalytic rate on catalyst potential V_{WR} or, equivalently (3, 28, 29), change $\Delta(e\Phi)$ in catalyst work function $e\Phi$. The rate exhibits "inverted-volcano"-type behavior (16) with the minimum near to the open-circuit conditions. This type of behavior has also been observed in several previous electrochemical promotion studies

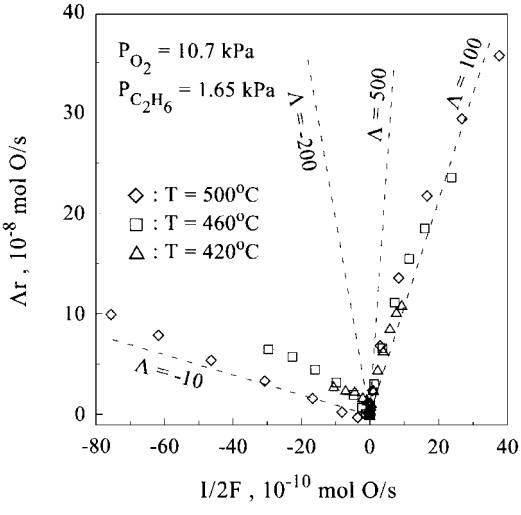

FIG. 7. Effect of the rate, $I/2F$, of electrochemical oxygen ion supply ($I>0$) or removal ($I<0$) on the induced increase in the rate of C_2H_6 oxidation.

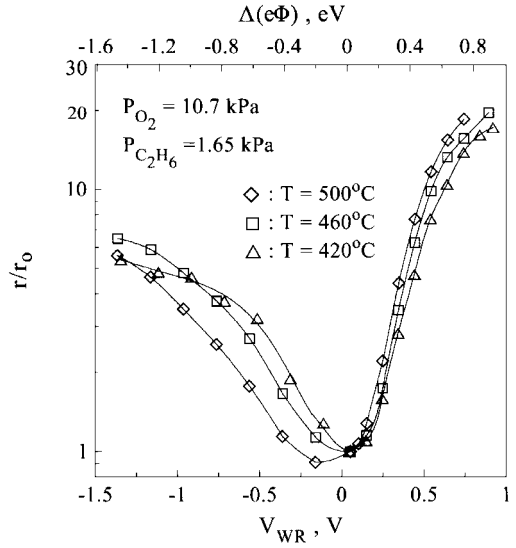

FIG. 8. Effect of catalyst potential and work function change on the rate enhancement ratio $\rho(=r/r_o)$ at fixed gaseous composition. The open-circuit rate, r_o, equals 0.68×10^{-8}, 1.27×10^{-8}, and 2.04×10^{-8} mol O/s at $T = 420$, 460, and 500°C, respectively.

of catalytic oxidations on Pt/YSZ (15–17) and Ag/YSZ (15–17).

For positive potentials the reaction exhibits electrophobic behavior and in the range $0.15\ \text{V} < V_{\text{WR}} < 0.5\ \text{V}$ the rate increases exponentially with catalyst potential and work function according to

$$\ln(r/r_o) = \alpha(e\Phi - e\Phi^*)/k_b T, \qquad [16]$$

where k_b is Boltzmann's constant and the parameter α, termed NEMCA coefficient (15–17), is of the order of 0.35 in this region. This exponential-type rate dependence on catalyst potential and work function has also been observed in numerous previous NEMCA studies (15–17).

For negative potentials the reaction exhibits electrophilic behavior and Eq. [16] is again approximately satisfied with α values near -0.1.

By comparing Figs. 6 and 8, one can observe that the potential—or overpotential—ranges where the exponential rate vs potential relationship holds (Eq. [16]) coincide with the ranges where the exponential current vs potential dependence is valid.

Figure 9a shows the effect of catalyst potential V_{WR} on the reaction kinetics with respect to P_{O_2}. Two observations can be made: (a) the rate is enhanced with both positive and negative potentials and (b) the P_{O_2} value at the rate maximum, $P^*_{O_2}$, increases significantly with increasing V_{WR} and decreases with decreasing V_{WR} (Fig. 9b). These observations indicate that increasing V_{WR}, and catalyst work function $e\Phi$, weakens significantly the chemisorptive bond of oxygen as in all previous electrochemical promotion studies of catalytic oxidations (15–17). As shown in Fig. 9b, $P^*_{O_2}$ increases by a factor of eight upon increasing V_{WR} by 1.5 V. Interestingly the variation is near linear.

Figure 10 shows the effect of catalyst potential V_{WR} on the reaction kinetics with respect to ethane. It is worth noting that: (a) positive potentials significantly enhance the rate and decrease the apparent order of the reaction with respect to $P_{C_2H_6}$, the latter indicating enhanced binding of ethane on the surface at high potentials where the rate dependence on $P_{C_2H_6}$ parallels that of a Langmuir adsorption isotherm, and (b) negative potentials enhance the rate only for low $P_{C_2H_6}$ values. Under such low $P_{C_2H_6}/P_{O_2}$ values the rate is negative order in oxygen (Fig. 3).

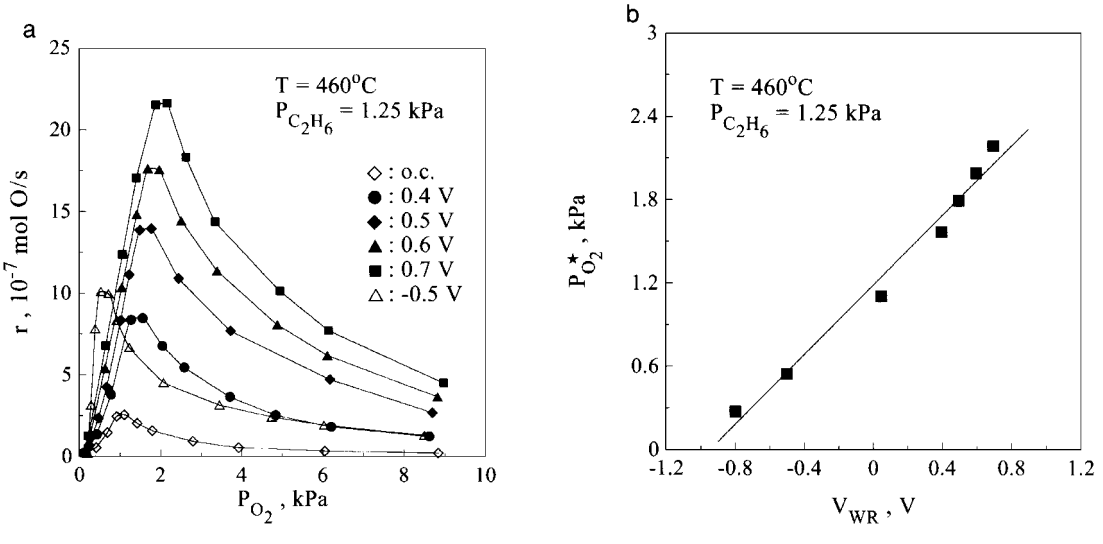

FIG. 9. (a) Effect of P_{O_2} on the rate of C_2H_6 oxidation under open-circuit (o.c.) conditions and at various imposed catalyst potentials. (b) Effect of imposed catalyst potential on the P_{O_2} value, $P^*_{O_2}$, which maximizes the rate.

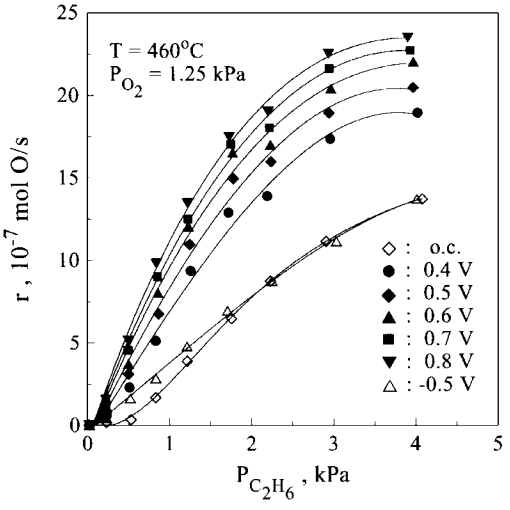

FIG. 10. Effect of $P_{C_2H_6}$ on the rate of C_2H_6 oxidation under open-circuit (o.c.) conditions and at various imposed catalyst potentials.

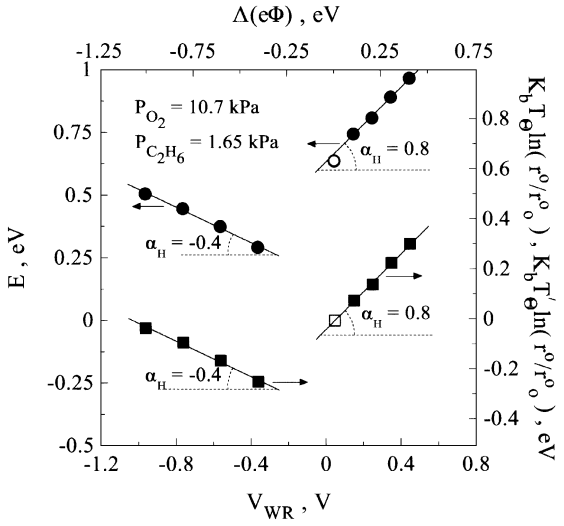

FIG. 12. Effect of catalyst potential and work function on the apparent activation energy, E, and on the logarithm of the preexponential factor r^o; r^o_o is the open-circuit preexponential factor and T_Θ, T'_Θ are the isokinetic points for positive and negative potentials, respectively.

Effect of Catalyst Potential on the Catalytic Activation Energy

Figures 11a and 11b show Arrhenius plots obtained at various fixed values of catalyst potential and compare them with the open-circuit (o.c.) Arrhenius plot. Figure 11a refers to positive potentials and Fig. 11b to negative ones. In both cases compensation effect behavior is obtained (43, 44). In the former case all Arrhenius lines corresponding to a fixed potential converge to a single isokinetic point, $T_\Theta = 230°C$. In the latter case again all the fixed potential Arrhenius lines converge to a second isokinetic point $T'_\Theta = 294°C$.

It is worth noting that the open-circuit Arrhenius line does not pass from any of the two isokinetic points. This must be because in open-circuit operation the catalyst potential is not fixed to a specific value but varies somewhat with temperature (between −0.1 and +0.05 V).

Figure 12 shows the dependence of the apparent activation energy values, E, extracted from the Arrhenius plots of Figs. 11a and 11b, on the catalyst potential V_{WR}. Interestingly the E vs V_{WR} dependence parallels the r vs V_{WR} dependence (Fig. 7), i.e., E exhibits a minimum near the open-circuit conditions. In the electrophobic region

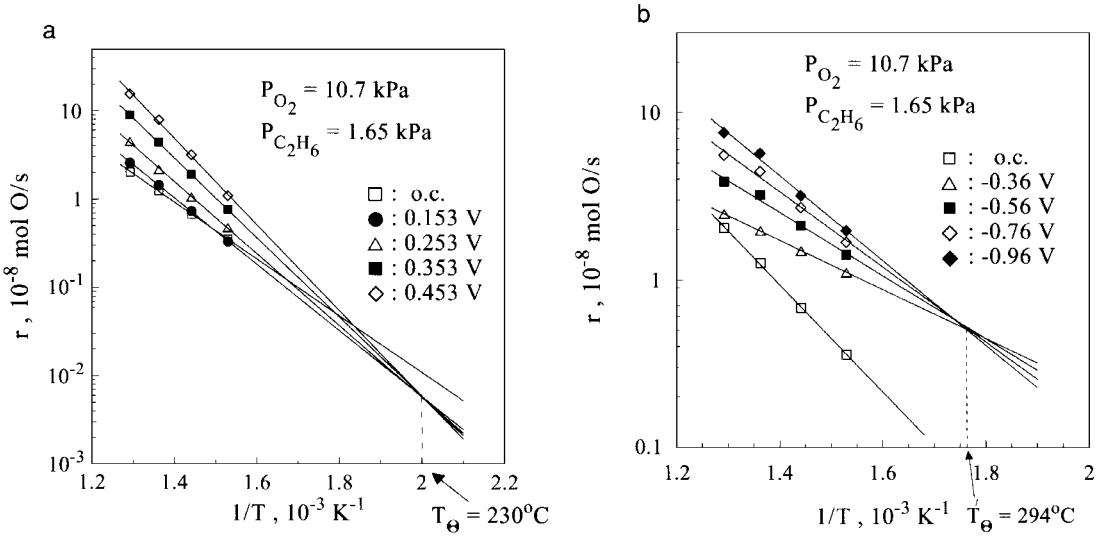

FIG. 11. Promotionally induced compensation effect. Arrhenius plots at various fixed positive (a) and negative (b) catalyst potentials; comparison with the open-circuit (o.c.) Arrhenius plot.

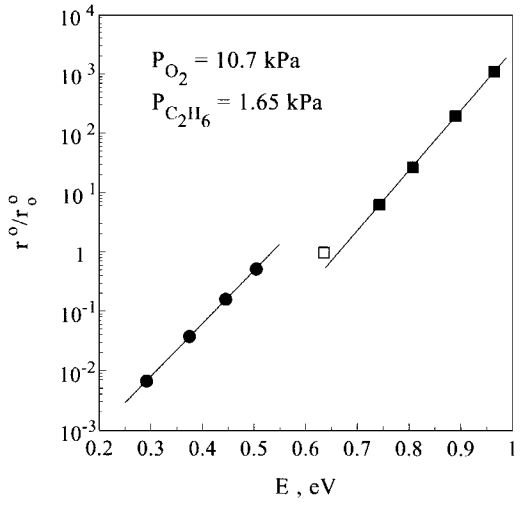

FIG. 13. Effect of the apparent activation energy, E, on the apparent preexponential factor, r^o, at various fixed positive (squares) and negative (circles) potentials; open symbol corresponds to open-circuit conditions.

$(\partial r/\partial V_{WR} > 0)$ the activation energy E increases linearly with V_{WR} (and $e\Phi$) with a slope $\alpha_H = 0.8$:

$$\Delta E = \alpha_H \Delta(e\Phi). \qquad [17]$$

In the electrophilic region $(\partial r/\partial V_{WR} < 0)$ the activation energy E conforms again to Eq. [14] with $\alpha_H = -0.4$. It is worth noting that E in the electrophobic region is significantly higher than in the electrophilic one.

The apparent preexponential factor r^o, defined from

$$r = r^o \exp(-E/k_b T), \qquad [18]$$

parallels the activation energy behavior (Fig. 12). Its logarithm varies linearly with V_{WR} and in fact when plotted as $k_b T_\Theta \ln(r^o/r_o^o)$, where T_Θ (or T'_Θ) is the isokinetic point, and r_o^o is the open-circuit preexponential factor, one obtains the same functional dependence on V_{WR}, as the E dependence on V_{WR}, diplaced vertically by the open-circuit activation energy E_o (Fig. 12).

This is because, as shown previously (19), when an isokinetic point exists, then E and $\ln r_o$ are related via

$$E - E_o = k_b T_\Theta \ln\left(r^o/r_o^o\right). \qquad [19]$$

Equation [19] is satisfied for every V_{WR} value and consequently when $\ln(r^o/r_o^o)$ is plotted vs E two straight lines are obtained with slopes $k_b T_\Theta$ and $k_b T'_\Theta$, respectively as shown in Fig. 13.

DISCUSSION

The present work shows that the catalytic activity of Pt for ethane oxidation can be markedly affected via the NEMCA effect by using Y_2O_3-stabilized zirconia-ZrO_2 as an active catalyst support and promoter donor. Similarly to the case of C_2H_4 oxidation on Pt/YSZ (2), Pt/β''-Al_2O_3 (4) and Rh/YSZ (19) the reaction is strongly electrophobic at high potentials; i.e., the rate increases significantly with O^{2-} supply to the catalyst. The maximum observed catalytic rate enhancement in this region ($\rho = r/r_o \approx 20$) is a factor of three lower than the maximum ρ value ($\sim$60) measured with C_2H_4 oxidation on Pt/YSZ.

All the observed features of electrochemical promotion in this region, i.e., the order of magnitude of $\Lambda(\sim 2Fr_o/I_o)$ and of τ $(\sim 2FN/I)$, are consistent with the electrochemically controlled oxide ion backspillover promoting mechanism (1, 15–17) now strongly supported by XPS (21–23), SERS (24, 25), TPD (26), cyclic voltammetry (26), and STM (27).

Interestingly in the present case ethane oxidation is also found to exhibit a rather strong electrophilic behavior ($\rho \sim 7$) at low potentials, i.e., with electrochemical removal of oxygen from the Pt surface. Clearly this type of electrophilic electrochemical promotion, also observed in the cases of CO oxidation on Pt/YSZ (15, 16) and Ag/YSZ (15, 16) and of C_3H_6 oxidation on Pt/YSZ (39), is not due to oxide ion backspillover, since oxygen is in this case being removed electrochemically from the Pt surface. That the promoting mechanism in this region, of negative currents and low potentials, is different from that in the region of positive currents and high potentials is also manifest by the pronounced minima in reaction rate and activation energy near the open-circuit conditions (Figs. 8 and 12) and also by the appearance of two different isokinetic points (Figs. 11a and 11b).

The observed compensation effect (42, 43) shows, in conjunction with other recent similar results (15–17), that the promotion-induced compensation effect is a rather common phenomenon resulting from the linear variation of activation energy and logarithm of preexponential factor with catalyst potential and work function (Fig. 12).

Origin of the Promoting Action

As previously noted it is now well established that when using YSZ and positive currents, the NEMCA effect is due to the promotional action of backspillover oxide ions $O^{\delta-}$ (O1*s* binding energy at 528.8 eV (21) peak desorption temperature $T_p \sim 750$–780 K (26)) which spread over the entire catalyst surface, increase its work function by

$$\Delta(e\Phi) = e\Delta V_{WR}, \qquad [5]$$

and act as sacrificial promoters by reacting with ethane at a rate Λ times smaller than the displaced (26) more weakly bonded atomic oxygen ($T_p \sim 675$–685 K).

It is worth emphasizing that Eq. [5] is also valid when applying negative currents, i.e., in the low-catalyst potential region as well. Also in both regions the Helmholz equation

is valid (15–17),

$$e\Delta V_{WR} = \Delta(e\Phi) = -\frac{eN_m}{\varepsilon_o}\sum_j \Delta(\mu_j \cdot \theta_j), \qquad [20]$$

where N_m is the surface metal atom concentration (e.g., 1.53×10^{19} atom/m^2 for Pt(111)) $e = 1.6 \times 10^{-19}$ C/atom, $\varepsilon_o = 8.85 \times 10^{-12}$ C^2/J · m and μ_j stands for the (average) dipole moment of all species j present on the catalyst surface at a coverage θ_j. When applying positive currents and thus increasing V_{WR} in the Pt/YSZ system, the increase in $e\Phi$ is accommodated primarily by the increase in the coverage of the backspillover oxide ions $O^{\delta-}$ whose dipole moment is expected to be higher than that of other covalently bonded species (e.g., coadsorbed atomic oxygen and ethane). However, changes in the coverages and dipole moments of these coadsorbed species are also quite possible, as actually manifest in TPD studies of oxygen on Pt/YSZ (26) where significant changes in the chemisorptive state of coadsorbed atomic oxygen was observed (27).

When using negative currents in the Pt/YSZ system, there can be no backspillover oxide migration to the catalyst surface, only chemisorbed oxygen removal, and thus the Helmholz equation [20] has to be accommodated only by changes in the coverages and dipole moments of dissociatively chemisorbed oxygen and C_2H_6. A decrease in oxygen coverage will in general cause a decrease in $e\Phi$ (15–17). A decrease in dipole moment μ due to tighter binding of oxygen on the Pt surface will also cause the same effect. As manifest in Fig. 9 negative potentials cause a decrease in $P^*_{O_2}$, thus a strengthening of the Pt=O bond, as expected for electron donor adsorbates, such as atomic oxygen, upon decreasing the catalyst work function (15–17). Consequently one can attribute the electrochemical promotional action in the region of negative currents (and low potentials) to Eq. [5] in conjunction with the Helmholz equation [20], i.e., to the fact that a decrease in potential forces a tighter binding of dissociatively chemisorbed oxygen, and weaker binding of dissociatively chemisorbed C_2H_6 on the Pt surface (15–17) with a concomitant readjustment in surface coverages of oxygen and C_2H_6 in order to satisfy Eq. [5].

One can thus rationalize all the observed promotional features on the reaction kinetics with respect to P_{O_2} (Fig. 9) and $P_{C_2H_6}$ (Fig. 10) in terms of the following simple rule used to explain all previous NEMCA studies. Increasing catalyst work function, either via the action of backspillover ions or via readjustment in surface coverages and dipole moments due to the applied potential, causes a weakening in the chemisorptive bond strength of dissociatively chemisorbed oxygen (electron acceptor) and a strengthening in the chemisorptive bond strength of dissociatively chemisorbed C_2H_6 (electron donor). This causes both the increase in $P^*_{O_2}$ (Fig. 9) and the decrease in apparent reaction order with respect to C_2H_4 (Fig. 10) with increasing V_{WR} and $e\Phi$.

Activation Energy Dependence on Work Function and Compensation Effect

The above simple promotional rule can also explain the observed peculiar dependence of the apparent activation energy on catalyst potential (Fig. 12).

We start the analysis by noting that the apparent activation energy of a bimolecular catalytic reaction

$$A + B \rightarrow C + D \qquad [21]$$

following Langmuir–Hinshelwood kinetics; i.e.,

$$r = k_R k_A k_B P_A P_B/(1 + k_A P_A + k_B P_B)^2 \qquad [22]$$

is given by the expression (5)

$$E = E_R - Q_A - Q_B + 2\frac{k_A P_A Q_A + k_B P_B Q_B}{1 + k_A P_A + k_B P_B}, \qquad [23]$$

where E_R is the true activation energy, k_A and k_B are the adsorption equilibrium constants of A and B, and Q_A, Q_B are the corresponding heats of adsorption of A and B. In the case of ethane oxidation and in view of the fact that the stoichiometry of the dissociative ethane chemisorption is not well known (37) one can write to a first approximation Eq. [23] as

$$E = E_R - Q_O - Q_{C_2H_6} + 2\frac{k_O P_{O_2}^{1/2} Q_O + k_{C_2H_6} P_{C_2H_6} Q_{C_2H_6}}{1 + k_O P_{O_2}^{1/2} + k_{C_2H_6} P_{C_2H_6}}. \qquad [24]$$

In view of the observed kinetic behavior (Figs. 9 and 10) it is reasonable to assume that $k_O P_{O_2}^{1/2} > 1$ and $k_{C_2H_6} P_{C_2H_6} > 1$, in which case Eq. [24] can be written as

$$E = E_R + \frac{k_O P_{O_2}^{1/2} - k_{C_2H_6} P_{C_2H_6}}{k_O P_{O_2}^{1/2} + k_{C_2H_6} P_{C_2H_6}}[Q_O - Q_{C_2H_6}]. \qquad [25]$$

We then note that, as previously discussed, Q_O is expected to decrease with increasing $e\Phi$, while $Q_{C_2H_6}$ is expected to increase. Assuming linear variations (30), i.e.,

$$Q_O = Q_O^o - \alpha_1 \Delta(e\Phi) \qquad [26]$$

$$Q_{C_2H_6} = Q^o_{C_2H_6} + \alpha_2 \Delta(e\Phi), \qquad [27]$$

where $\alpha_1, \alpha_2 > 0$, one can rewrite Eq. [25] as

$$E = E_R + \frac{k_O P_{O_2}^{1/2} - k_{C_2H_6} P_{C_2H_6}}{k_O P_{O_2}^{1/2} + k_{C_2H_6} P_{C_2H_6}} \times \left[Q_O^o - Q^o_{C_2H_6} - (\alpha_1 + \alpha_2)\Delta(e\Phi)\right]. \qquad [28]$$

This equation can be used in the attempt to rationalize the observed complex dependence of E on $\Delta(e\Phi)$ in a qualitative fashion. The sign of $\partial E/\partial(e\Phi)$ depends on the sign

of the parameter $A = k_O P_{O_2}^{1/2} - k_{C_2H_6} P_{C_2H_6}$. For high $\Delta(e\Phi)$ values oxygen adsorption is weakened and ethane adsorption is strengthened; A is thus negative and, according to Eq. [28], E increases linearly with $\Delta(e\Phi)$ as experimentally observed (Fig. 12). For negative $\Delta(e\Phi)$ values oxygen adsorption is strong and ethane adsorption is weak; thus A is positive and, according to Eq. [28], E increases linearly with decreasing $\Delta(e\Phi)$, again in good qualitative agreement with experiment (Fig. 12).

Transient Analysis and Promotion Index

As previously noted, determination of the promotion index $PI_{O^{\delta-}}$ of the promoting oxide ions $O^{\delta-}$ requires knowledge of the coverage of $O^{\delta-}$ on the catalyst surface. This can be done by using the rate transient analysis upon current interruption. We first consider the mass balance of $O^{\delta-}$ during current application ($0 \le t \le t_o$)

$$N_O \frac{d\theta_{O^{\delta-}}}{dt} = (I/2F) - N_O f(\theta_{O^{\delta-}}), \qquad [29]$$

where $f(\theta_{O^{\delta-}})$ is the rate of consumption of $O^{\delta-}$ on the catalyst surface, due to reaction with C_2H_6. We then note that in the region of positive potentials the catalytic rate is exponentially dependent on $\Delta(e\Phi)$ (Eq. [16], Fig. 8). The change in work function $e\Phi$, $\Delta(e\Phi)$, is linearly related to $\theta_{O^{\delta-}}$, provided the dipole moment of $O^{\delta-}$ is constant with coverage. On the basis of this assumption one can write

$$r = r_o \exp(\gamma \theta_{O^{\delta-}}), \qquad [30]$$

where γ is a constant. It follows then from Eq. [29] and the initial condition ($t = 0$, $\theta_{O^{\delta-}} = 0$) that

$$N_O \frac{d\theta_{O^{\delta-}}}{dt}\bigg|_{t=0} = N_O \frac{d\ln(r/r_o)}{dt}\bigg|_{t=0} = (I/2F)\gamma. \qquad [31]$$

Consequently γ can be obtained from the initial slope of $\ln(r/r_o)$ vs t. For the rate transient upon current imposition (Fig. 5a) one can estimate a γ value of 6.5.

We then note that as steady state it is

$$(I/2F) = N_O f(\theta_{O^{\delta-}}) \qquad [32]$$

and that, in view of Eq. [31],

$$N_O \frac{d\theta_{O^{\delta-}}}{dt}\bigg|_{t=t_o} = -N_O f(\theta_{O^{\delta-}}) = -(I/2F), \qquad [33]$$

where the last equality in [33] holds because of Eq. [32]. In view of Eq. [33] one has

$$N_O \frac{d\ln(r/r_o)}{dt}\bigg|_{t=t_o} = -\gamma(I/2F), \qquad [34]$$

which implies that a second estimate of γ can also be obtained from the initial rate slope upon current interruption. From the transient upon current interruption of Fig. 5a one obtains $\gamma = 5.6$, in reasonable agreement with the value estimated upon current imposition.

Once γ has been estimated, one can then compute $\theta_{O^{\delta-}}$ from Eq. [34] for any time t from the corresponding r/r_o value, i.e.,

$$\theta_{O^{\delta-}} = \frac{1}{\gamma}\ln(r/r_o) = -\frac{\ln(r/r_o)}{d\ln(r/r_o)/dt}(I/2FN_O). \qquad [35]$$

The maximum $\theta_{O^{\delta-}}$ value is thus computed for the transient of Fig. 5a to be $\theta_{O^{\delta-}} \approx 0.5$. This, in view of Eq. [4] and the observed ρ value ($\rho \approx 16.5$) gives a $PI_{O^{\delta-}}$ value of the order of 33 in good qualitative agreement with $PI_{O^{\delta-}}$ values for other Pt catalyzed oxidations [15–17].

CONCLUSIONS

Ethane oxidation on Pt films deposited on YSZ exhibits a rather strong electrochemical promotion effect at temperatures 400 to 500°C. Both positive and negative applied potentials enhance the rate of oxidation by up to a factor of 20 and 7, respectively. The rate increase is typically a factor of 200 to 20 higher than the rate of electrochemical supply or removal of oxygen, respectively. The reaction kinetics and apparent activation energy are also significantly modified by the applied potential leading to the appearance of the compensation effect. These modifications as well as the pronounced rate enhancement are consistent with the notion that increasing catalyst potential and work function weakens the chemisorptive bond strength of oxygen and enhances dissociative ethane chemisorption on the Pt surface while decreasing catalyst potential and work function has exactly the opposite effect.

The observed transient behavior with positive current application is in good agreement with the oxide-ion backspillover mechanism for electrochemical promotion and allows for the estimation of the coverage of the promoting oxidic backspillover species. The picture is still less clear regarding the promoting mechanism with negative currents, i.e., electrochemical oxygen removal from the catalyst surface. The use of surface spectroscopic techniques under such conditions could provide useful additional insight.

ACKNOWLEDGMENT

We thank the PENED Programme of the Hellenic Secretariat of Research and Technology for partial financial support.

REFERENCES

1. Vayenas, C. G., Bebelis, S., and Neophytides, S., *J. Phys. Chem.* **92**, 5083 (1988).
2. Bebelis, S., and Vayenas, C. G., *J. Catal.* **118**, 125 (1989).
3. Vayenas, C. G., Bebelis, S., and Ladas, S., *Nature (London)* **343**, 625 (1990).

4. Pritchard, J., *Nature (London)* **343**, 592 (1990).
5. Yentekakis, I. V., Moggridge, G., Vayenas, C. G., and Lambert, R. M., *J. Catal.* **146**, 293 (1994).
6. Vayenas, C. G., Bebelis, S., and Despotopoulou, M., *J. Catal.* **128**, 415 (1991).
7. Politova, T. I., Sobyanin, V. A., and Belyaev, V. D., *React. Kinet. Catal. Lett.* **41**, 321 (1990).
8. Makri, M., Buekenhoudt, A., Luyten, J., and Vayenas, C. G., *Ionics* **2**, (1996).
9. Tsiplakides, D., Neophytides, S., Enea, O., Jaksic, M. M., and Vayenas, C. G., *J. Electrochem. Soc.* [In press]
10. Yentekakis, I. V., and Vayenas, C. G., *J. Catal.* **149**, 238 (1994).
11. Pliangos, C., Yentekakis, I. V., Ladas, S., and Vayenas, C. G., *J. Catal.* **159**, 189 (1996).
12. Neophytides, S., Tsiplakides, D., Stonehart, P., Jaksic, M. M., and Vayenas, C. G., *Nature (London)* **370**, 45 (1994).
13. Neophytides, S. G., Tsiplakides, D., Stonehart, P., Jaksic, M. M., and Vayenas, C. G., *J. Phys. Chem.* **100**, 14803 (1996).
14. Anastasievic, N., and Werner, D., *in* "Proceedings, GDCh Angewandte Elektrochemie," Monheim, October 1996.
15. Vayenas, C. G., Bebelis, S., Yentekakis, I. V., and Lintz, H.-G., *Catal. Today* **11**, 303 (1992).
16. Vayenas, C. G., Jaksic, M. M., Bebelis, S., and Neophytides, S. G., *in* "Modern Aspects of Electrochemistry" (J. O'M. Bockris, B. E. Conway, and R. E. White, Eds.), Vol. 29, p. 57. Plenum Press, New York, 1995. [And references therein]
17. Vayenas, C. G., and Neophytides, S. G., *in* "Catalysis," Vol. 12, Chap. 6, p. 199. The Royal Society of Chemistry, Cambridge, UK, 1996.
18. Varkaraki, E., Nicole, E., Plattner, E., Comninellis, Ch., and Vayenas, C. G., *J. Appl. Electrochem.* **25**, 978 (1995).
19. Pliangos, C., Yentekakis, I. V., Verykios, X. E., and Vayenas, C. G., *J. Catal.* **154**, 124 (1995).
20. Marina, O., Yentekakis, I. V., Vayenas, C. G., Palermo, A., and Lambert, R. M., *J. Catal.* **166**, 218 (1997).
21. Ladas, S., Kennou, S., Bebelis, S., and Vayenas, C. G., *J. Phys. Chem.* **97**, 8845 (1993).
22. Palermo, A., Tikhov, M. S., Filkin, N., Lambert, R. M., Yentekakis, I. V., and Vayenas, C. G., *Stud. Surf. Sci. Catal.* **101**, 513 (1996).
23. Arakawa, T., Saito, A., and Shiokawa, J., *Chem. Phys. Lett.* **94**, 250 (1983); *Appl. Surf. Sci.* **16**, 365 (1983).
24. Basini, L., Cavalca, C. A., and Haller, G. L., *J. Phys. Chem.* **88**, 10853 (1994).
25. Kondarides, D. I., Papatheodorou, G. N., Vayenas, C. G., and Verykios, X. E., *Ber. Bunsenges. Phys. Chem.* **97**, 709 (1993).
26. Neophytides, S., and Vayenas, C. G., *J. Phys. Chem.* **99**, 17063 (1995).
27. Makri, M., Vayenas, C. G., Bebelis, S., Besocke, K., and Cavalca, C. A., *Surf. Sci.* **369**, 351 (1996).
28. Ladas, S., Bebelis, S., and Vayenas, C. G., *Surf. Sci.* **251/252**, 1062 (1991).
29. Zipprich, W., Wiemhöfer, H.-D., Vohrer, U., and Göpel, W., *Ber. Bunsenges. Phys. Chem.* **99**, 1406 (1995).
30. Pacchioni, G., Ilas, F., Neophytides, S., and Vayenas, C. G., *J. Phys. Chem.* **100**, 16653 (1996).
31. Yao, Y.-F. Y., and Kummer, J. T., *J. Catal.* **28**, 124 (1973).
32. Fairbridge, C., and Ross, R. A., *Can. J. Chem.* **60**, 893 (1982).
33. Wachs, I. E., and Kelemen, S. R., *J. Catal.* **68**, 213 (1981).
34. Erdöhelyi, A., and Solymosi, F., *J. Catal.* **123**, 31 (1990).
35. Oyama, S. T., Middlebrook, A. M., and Somorjai, G. A., *J. Phys. Chem.* **94**, 5029 (1990).
36. Harold, M. P., and Luss, D., *Ind. Eng. Chem. Res.* **26**, 2092 (1987). [And references therein]
37. McMaster, M. C., and Madix, R. J., *Surf. Sci.* **275**, 265 (1992).
38. Liu, A. C., and Friend, C. M., *Surf. Sci.* **216**, 33 (1989).
39. Kaloyannis, A. C., Pliangos, C. A., Yentekakis, I. V., and Vayenas, C. G., *Ionics* **1**, 159 (1995).
40. Yentekakis, I. V., and Bebelis, S., *J. Catal.* **137**, 278 (1992).
41. Cavalca, C. A., Larsen, G., Vayenas, C. G., and Haller, G. L., *J. Phys. Chem.* **97**, 6115 (1993).
42. Karavassilis, Ch., Bebelis, S., and Vayenas, C. G., *J. Catal.* **160**, 190, 205 (1996).
43. Cremer, E., *Adv. Catal.* **7**, 75 (1955).
44. Schwab, G.-M., *J. Catal.* **84**, 1 (1983).